SIMFONY: Multiplexed Single-Inductor Multi-Function 1.2 µW Standby Health Monitoring Node with HBC, SIMO, PPG, and Inference

Anhang Li[1,2], Junyi Luo[2], Ruichen Qi[2], Hongyi Wu[1], Dennis Sylvester[1], Mehdi Saligane[2]
[1] University of Michigan, Ann Arbor, MI, USA
[2] Brown University, Providence, RI, USA

***Abstract*—This paper presents SIMFONY, a health-monitoring system based on the Single Inductor Multiple Function technique. It enables key functionalities, including high-efficiency human body communication (HBC) at 8.9pJ/b system-level; with an underlying resonance, TX block achieves 2.8 pJ/b; a wakeup radio; Li-ion cell to 0.6V and 1.2V power rails conversion (SIMO) with 85% peak efficiency; and a voltage-boosting, constant-current LED driver delivering up to 150mA for photoplethysmogram (PPG) applications. These functions are achieved with only one high-voltage (HV) tolerant node and by reusing HV switches across operating modes. Finally, together with an on-chip inference engine, SIMFONY demonstrates a proof-of-concept biosignature-based key generation for encryption across multiple body locations.**

***Index Terms*—Human body communication (HBC), Wearable health monitoring, SIMO**

I. Introduction

Secure, continuous collection of physiological data can enable personalized models for wellness monitoring and early detection, ultimately paving the way toward proactive and data-driven healthcare. This work targets a compact biosensing platform capable of long-term data collection, communication, and local processing under severe size and battery-life constraints [1] (Fig. 1). Such a platform needs to support sensor interfaces, communication, and on-chip inference simultaneously, with long standby battery life. This paper proposes SIMFONY, which combines five functions: HBC TX, HBC RX, WUR, SIMO power conversion, and PPG LED driving by time-multiplexing a single inductor and reusing key switching and resonant components. This technique extends the single-inductor, multiple-output (SIMO) concept introduced in [2] to additional non-power functions (i.e. HBC and sensing) enabled by a dedicated arbitration mechanism and validated by measurements.

II. Proposed Inductor-Based Architecture

HBC application operates with human skin: a capacitive load with an appropriate electrode design. As shown in Fig. 2, prior arts have explored the possibility of inductive resonating with the capacitance to achieve passive gain RX, and low power TX [3]. Surveys have shown that $10kHz \sim 35MHz$ is a suitable band for HBC communication [4], with $5MHz$ yielding the lowest loss [5]. Accordingly, $L = 15\mu H$ is selected.

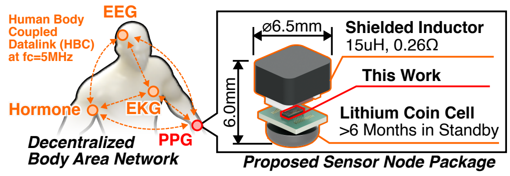

Fig. 1. Intended Wearable Health-Monitoring Application

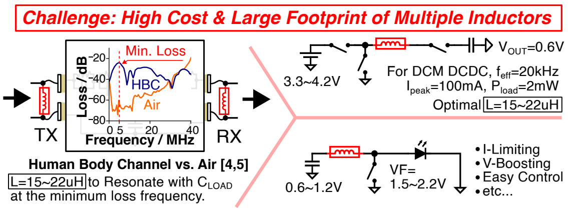

Fig. 2. Use of Inductor in Efficient Power, LED Driver, and HBC Circuits

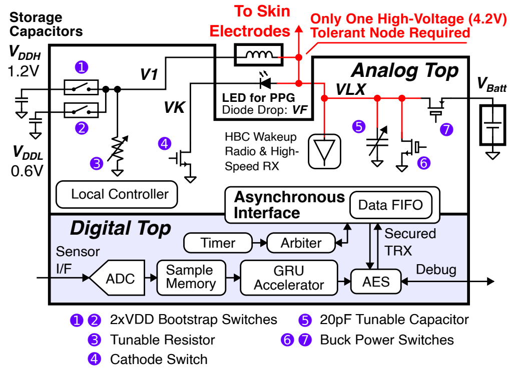

Fig. 3. Proposed Single-Inductor PPG + HBC + Edge-ML Circuit

Next, Fig. 2 highlights two major power conversion step required by such a bio-sensing platform: buck conversion from a lithium-ion battery to the required $0.6V$ core voltage; and a boosting converter required for driving an LED. They can be implemented efficiently with a inductor. $L = 15\mu H$ achieves a good balance of operating frequency and output power.

In summary, a discrete inductor is a key enabler for low-loss, high-energy-density power conversion, but it is also one of the bulkiest components in miniature wearable systems. To resolve this issue, we propose a inductor-sharing system. Fig. 3 shows a high-level diagram of the system, along with numeral callouts for circuit descriptions in later sections of this paper.

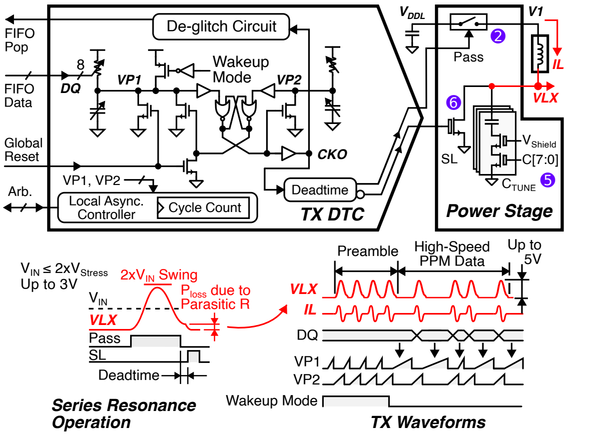

Fig. 4. Body-Coupled Communication Transmit (HBC-TX) Mode

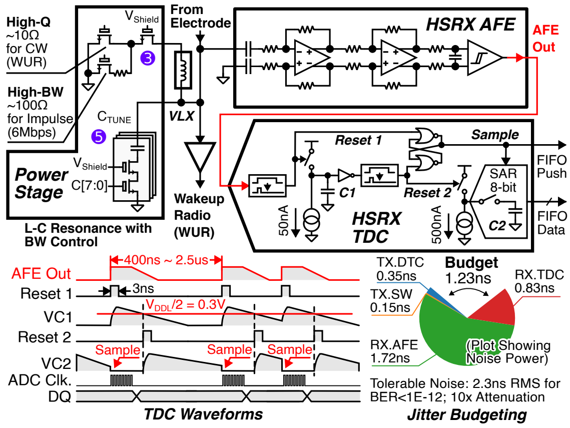

Fig. 5. Body-Coupled Communication Receive (HBC-RX) Mode

III. Circuit Implementation

A. HBC Transmitter (TX) mode

The HBC-TX mode (Fig. 4) operates in a novel series-resonance mode, with the inductor resonating with the load capacitance (primarily from the electrode-human skin interface) to produce single cosine pulses for a 6-bit-per-pulse (6bpp) pulse-position modulation (PPM) datalink [6], [7]. To enable low-power wakeup radio receivers, each data burst begins with a continuous wave (CW) preamble.

The inductive resonant circuit has multiple advantages, including state-of-the-art power efficiency ($2.8pJ/b$), up to 2xVDD ($> 4V$) amplitude, and an inherent bandwidth limitation that reduces out-of-band air emission. To maximize TX amplitude, 2×VDD-capable bootstrapping switches [8] (①, ②) are employed as high-speed pass-gate elements, turning on in $< 1ns$ to minimize loss. In contrast, the pull-down switch ⑥ has much relaxed timing requirements ($> 400ns$) and can be implemented with a small thick-gate transistor for high-voltage tolerance and low capacitive loading. A $20pF$ tunable capacitor ⑤ is added for frequency trimming.

B. HBC High-Speed Receiver (HSRX) and Wakeup Radio (WUR) Modes

The high-speed HBC receiver (HSRX) and wakeup radio (WUR) modes [9] (Fig. 5) reuse the inductor as a part of a shared input band-pass filtering circuit. In HSRX mode, the resonator Q is reduced to meet bandwidth requirements, whereas WUR benefits from a high-Q resonator to passively amplify the CW wakeup tone. A tunable resistor ③ adjusts the effective Q to support both modes.

Measurements show that short-term resonant frequency drift due to capacitance variation within a TX burst is $< 1ns$ RMS; however, burst-to-burst peak amplitude variation can still introduce $> 4ns$ timing error with naive detection. To reduce amplitude sensitivity, the tunable capacitor ⑤ is reused to implement a tuned high-pass-filter-based peak-to-zero-crossing conversion, similar to a laser range-finding application, reducing timing error to $< 1.2ns$ RMS at a cost of 3dB SNR [10]. The PPM pulses generated by the TX DTC circuit are digitized by an RX TDC circuit into the payload (Fig. 5).

C. LED Driver Mode

Many biomedical sensors use LEDs for illumination; in particular, photoplethysmography (PPG) uses LEDs with VF up to 3.4V, requiring voltage boosting, high peak current, and amplitude-controlled current. The proposed design uses an inductor-based boost-converter approach [11], [12] (Fig. 6) instead of relying on an external HV source like prior arts. Peak current is controlled by the on-time of charging switch ⑥, with $dI = (V_{DDL}/L)dt$. By controlling the on-time with a synchronous counter, the LED peak current is controlled by the switch's on-time.

D. SIMO Mode

Converting from a commonly used $3.3 \sim 4.2V$ lithium-based chemistry battery to the $0.6 \sim 1.2V$ supply voltage using an LDO would yield very poor conversion efficiency ($< 18\%$). A SIMO DC-DC converter with two outputs is used instead (Fig. 7) to generate these supply rails.

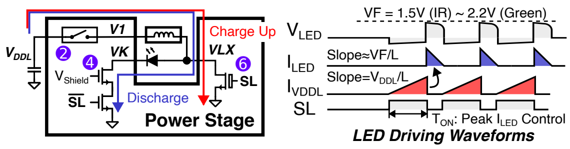

Fig. 6. High Efficiency LED Driver Mode

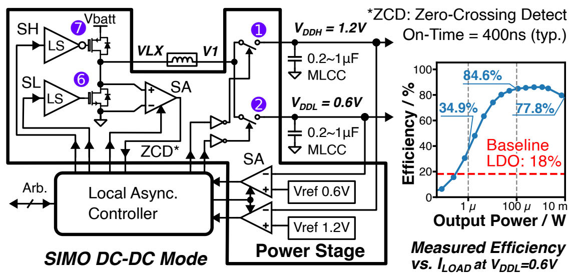

Fig. 7. SIMO DC-DC Converter Mode

The converter operates in DCM, with the output current optimized for $10\mu A \sim 2mA$ to cover the operating range of all other blocks, particularly the voltage-scaled RNN accelerator (Fig. 8) with up to $2mA$ peak current. In standby mode, where everything is turned off, the converter can achieve 34.9% efficiency — a near 2x improvement over LDOs. The DC-DC design can be built by sharing the existing elements: specifically, ⑥ serves as the input pull-down switch, while ① and ② are the output switches.

E. On-Chip Inference Engine

Instead of transmitting raw data directly, on-device processing reduces the amount of data need to transmit, and also allows us to perform data encryption before TX. Fig. 8 shows an on-chip inference engine integrating multi-sensor aggregation buffer, a GRU-based RNN accelerator, followed by an AES encryption engine.

With constant memory, our memory–accuracy trade-off experiment indicates that 6-bit quantization achieves the highest accuracy (98%) with 22k parameters when trained on the MIT-BIH [13] dataset. So internally the pipeline is quantized to 6-bits.

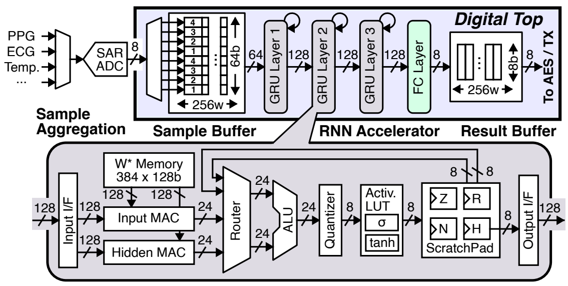

Fig. 8. Aggregated On-Chip Inference Pipeline

F. Time-Multiplexed Operation

Treating the inductor as a shared resource; a round-robin arbiter controls the 5 modes. (Table. I) The RX need to preemptively acquire the resource or incoming data will be lost. So HSRX is assigned the highest priority, and activated immediately when a wakeup call is detected. A measured example in Fig. 9 shows how the arbiter automatically replenishes VDDL after LED operation, and later transmits a preamble, followed by a payload after 1k ADC samples.

Combining multiple modes of operation requires careful mitigation of high-voltage hazards, which can otherwise damage thin-gate transistors. In the 65nm GP process, the breakdown voltage of a thin-gate transistor is 1.2V. Thanks to the topology, only the node between the inductor and battery

TABLE I
MULTI-TASK INDUCTOR ARBITER CONFIGURATION

	Priority	Function	Requester	Acknowledger	Next State
High	0	HBC HSRX	N/A	TDC Timeout	Release
	1	LED Pulse	Timer interrupt	LED Pulse Counter	Release
	2	HBC TX	Digital Top	Transmit Byte Counter	Release
	3	SIMO Channel 0	SIMO Comparator	ZCD	Release
	4	SIMO Channel 1	SIMO Comparator	ZCD	Release
Low	5	Wakeup Radio	Always 1	WUR Timeout or Wakeup signal received	Go to HSRX if awake

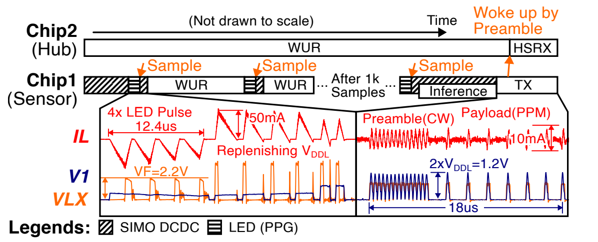

Fig. 9. Measured Example of Multiple Tasks Running Autonomously under Arbiter's Control

is exposed to HV (Fig. 3). More importantly, the HBC TX passgates with high-speed switching requirements (①, ②) are not connected to this node. This isolation enables simultaneous high-speed data transmission and HV power conversion. Shielding transistors have been added to all circuits near this node, providing up to 4.8V of high-voltage tolerance. All data receiving amplifiers (HSRX and WUR) are AC-coupled with MIM capacitors with sufficient voltage tolerance. Simulations have shown that the thin-gate input transistors will not exceed $VGS > 2V$ during power conversion.

IV. MEASUREMENTS

Fig. 10 showcases the measured waveforms of a proof-of-concept application enabled by SIMFONY. Using the integrated LED driver, the chip acquires PPG signals from multiple body sites, processes them with the on-chip inference engine, and derives an encryption key from spatially correlated physiological features. The proposed method generates one 128-bit per 47.41 s (2.70 bit/s) with BER $< 10^{-3}$, outperforming heartbeat-per-bit physiological key generators in throughput reported in prior ECG-based key-generation schemes [14]. Compared to ECG-based key generation, the method is more practical for wearable use because PPG can be acquired optically from many body locations where blood flow is available, whereas ECG generally relies on skin-contact bio-potential electrodes. [15]

Fig. 11 showcases additional performance measurement plots, including (a) HBC RX sensitivity; (b) DC-DC startup

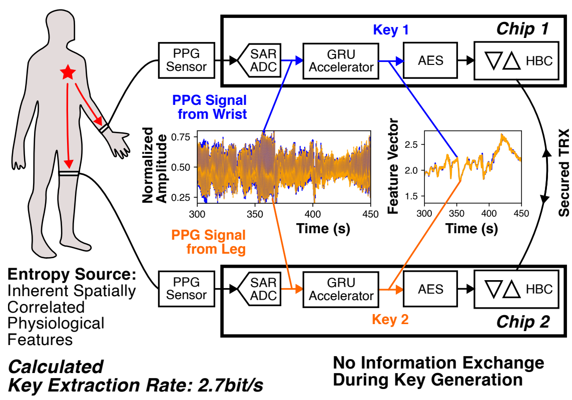

Fig. 10. Bio-Security Application Example

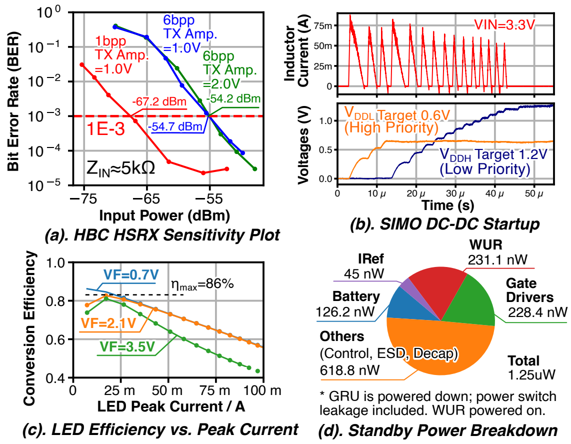

Fig. 11. Circuit Measurements

waveforms; (c) LED efficiency vs. peak inductor current; and (d) a breakdown of standby power.

V. Summary

This paper presents SIMFONY, a compact wearable health-monitoring chip that reuses a single inductor for HBC communication, wake-up reception, SIMO power conversion, and PPG LED driving, while also supporting on-chip inference and AES-based biometric key generation. It achieves $1.2\mu W$ standby power, $8.9pJ/b$ HBC TRX efficiency, 85% peak DC-DC efficiency, and up to $150mA$ LED drive capability. Fig. 13 compares each individual function with recent works [3], [6], [12], [16]–[18], showing that the overhead of inductor sharing remains modest such that the multiplexed system still maintains competitive performance. Fig. 12 shows the $2mm^2$ test chip fabricated in 65nm GP process, assembled with the external $15\mu H$ inductor on a PCB.

Acknowledgment

The authors would like to thank Google for their support.

References

[1] J. Kim *et al.*, "Wearable biosensors for healthcare monitoring," *Nature Biotechnology*, vol. 37, no. 4, pp. 389–406, Apr. 2019.

[2] D. Ma *et al.*, "Single-inductor multiple-output switching converters with time-multiplexing control in discontinuous conduction mode," *IEEE Journal of Solid-State Circuits*, vol. 38, no. 1, pp. 89–100, 2003.

[3] N. Modak *et al.*, "A 65nm resonant electro-quasistatic 5–240μw human whole-body powering and 2.19μw communication soc with automatic maximum resonant power tracking," in *IEEE Custom Integrated Circuits Conference (CICC)*, 2021, pp. 1–2.

[4] S. Maity *et al.*, "Bio-physical modeling, characterization, and optimization of electro-quasistatic human body communication," *IEEE Transactions on Biomedical Engineering*, vol. 66, no. 6, pp. 1791–1802, 2019.

[5] K. Hachisuka *et al.*, "Development of wearable intra-body communication devices," *Sensors and Actuators A: Physical*, vol. 105, no. 1, pp. 109–115, Jun. 2003.

[6] B. Chatterjee *et al.*, "A 65nm 63.3μw 15mb/s transceiver with switched-capacitor adiabatic signaling and combinatorial pulse-position modulation for body-worn video-sensing ar nodes," in *IEEE International Solid-State Circuits Conference (ISSCC)*, 2022, pp. 276–278.

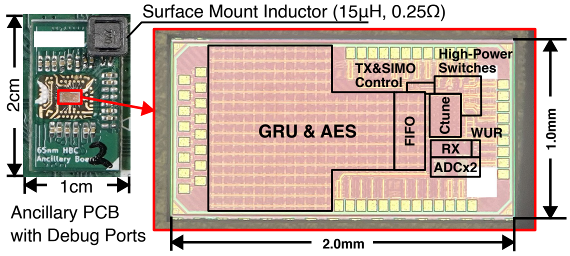

Fig. 12. Test Chip & Package Photograph

(a). HBC Comparison Table

Paper	This Work	[6]	[3]
Technique	Inductor Reson.	Switched Capacitor	Inductor Reson.
Demod. Method	TDC + DTC	CDR	CDR
Carrier Freq.	5MHz	20MHz	0.5~2MHz
WUR	Yes	No	No
Data Rate (bps)	6M	7.5~15M	1~20k
Maximum TX Amp.(V)	1.5 (V_{DD}@0.8V) 4.8 (V_{DD}@2.5V)	0.7	10
Best TX Efficiency (pJ/b)	2.8 1.0Vpp PPM 6 bpp	4.2 CPPM-6b	169
Best RX Efficiency (pJ/b)	6.1 PPM 6 bpp	4 CPPM-6b	3.6 OOK
TX Power	16.8 uW	63 uW	1.5 uW
RX Power	30.6 uW	60 uW	72 uW
Area (mm^2)	RX+WUR: 0.05 TX: 0.08	0.259	0.13
Sensitivity (dBm)	-67 (1bpp) -54 (6bpp) @1E-3 BER	-65 (OOK) -52 (CPPM) @1E-3 BER	-60 @1E-5 BER

(b). Li-Ion Capable SIMO Buck DC-DC Comparison Table

Paper	This Work	[16]	[17]
Inductance (H)	15u	10u	2.2u
Capacitor (F)	480n	20n	4.7u
V_{IN} (V)	1.5~4.2	3.8~4.4	2.8~3.3
V_{OUT} (V)	0.6~3.8	0.5~1.8	0.8~1.8
Peak PCE	85%	72.8%	95%
PCE @ 1uW	34%	-	<10%
Max P_{OUT} (W)	20m	960u	925m
leakage	<1uW	-	-

(c). Micro-Power PPG LED Driver Comparison Table

Paper	This Work	[12]	[18]
HV Source	Boost		External
VF Max (V)	4.5	>2.6	<5
ILED Max (A)	150m	100m	314m
Efficiency	79~86%	-	-
Current Control	On-Time + PDM	PDM	IDAC

Fig. 13. Comparison Tables

[7] A. Li *et al.*, "14-8: A 16nm 2.2pj/b high-efficiency pulse-position modulated resonance transceiver for 15mb/s multi-source high-speed body-area sensor networks," in *IEEE Custom Integrated Circuits Conference (CICC)*, 2026, in press.

[8] S. Lee *et al.*, "3.9 a 1.2v high-voltage-tolerant bootstrapped analog sampler in 12-bit sar adc using 3nm gaa 0.7v thin-gate-oxide transistor," in *IEEE International Solid-State Circuits Conference (ISSCC)*, 2024, pp. 70–72.

[9] V. Mangal and P. R. Kinget, "Sub-nw wake-up receivers with gate-biased self-mixers and time-encoded signal processing," *IEEE Journal of Solid-State Circuits*, vol. 54, no. 12, pp. 3513–3524, 2019.

[10] K. Li *et al.*, "A low walk error timing discrimination asic with rail-to-rail dynamic range and icmr for pulsed tof lidar receiver," *IEEE Transactions on Instrumentation and Measurement*, vol. 74, pp. 1–13, 2025.

[11] W. Saadeh, T. Tekeste, and M. H. Perrott, "A ¿89% efficient led driver with 0.5v supply voltage for low average current applications," in *IEEE Asian Solid-State Circuits Conference (A-SSCC)*, 2013, pp. 273–276.

[12] Q. Lin *et al.*, "A 119db dynamic range charge counting light-to-digital converter for wearable ppg/nirs monitoring applications," *IEEE Transactions on Biomedical Circuits and Systems*, vol. 14, no. 4, pp. 800–810, 2020.

[13] G. B. Moody and R. G. Mark, "The impact of the mit-bih arrhythmia database," *IEEE Engineering in Medicine and Biology Magazine*, vol. 20, no. 3, pp. 45–50, May–June 2001.

[14] Z. Zhang *et al.*, "Ecg-cryptography and authentication in body area networks," *IEEE Transactions on Information Technology in Biomedicine*, vol. 16, no. 6, pp. 1070–1078, 2012.

[15] T. Tamura, "Current progress of photoplethysmography and spo2 for health monitoring," *Biomed. Eng. Lett.*, vol. 9, no. 1, pp. 21–36, Feb. 2019.

[16] D. Kim *et al.*, "A 4.2-to-0.5 v, 0.8 μa–0.8 ma power-efficient three-level simo buck converter for a quad-voltage risc-v microprocessor," *IEEE Transactions on Very Large Scale Integration (VLSI) Systems*, vol. 33, no. 1, pp. 193–206, 2025.

[17] Y. Zhang *et al.*, "An adaptive zero-current detector for single-inductor multiple-output dc-dc converter with full-wave current sensor," *IEEE Transactions on Very Large Scale Integration (VLSI) Systems*, vol. 32, no. 9, pp. 1764–1768, 2024.

[18] V. R. Pamula *et al.*, "A 172 μw compressively sampled photoplethysmographic readout asic with heart rate estimation," *IEEE Transactions on Biomedical Circuits and Systems*, vol. 11, no. 3, pp. 487–496, 2017.